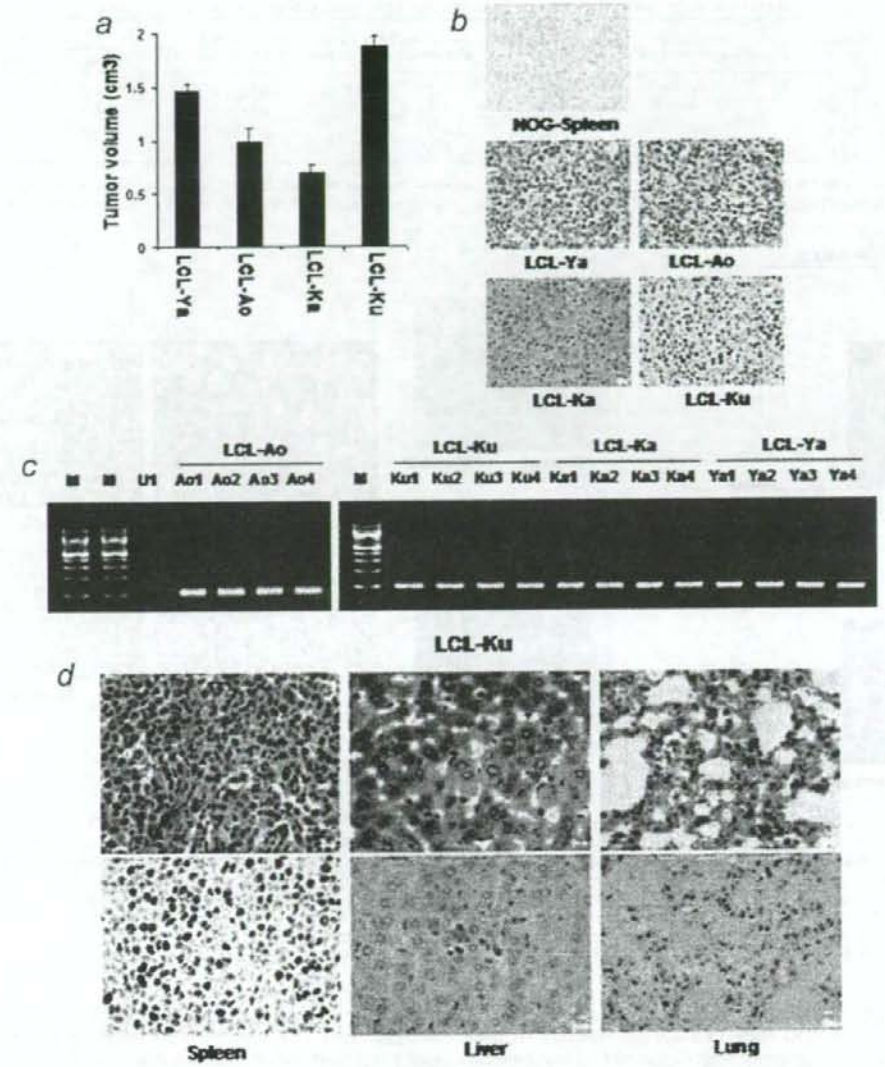

FIGURE 4 – Successful engraftment and infiltration of EBV-positive lymphoblastoid B cells in NOG mice. (*a*) Subcutaneous tumor size in mice 21 days after inoculation with various LCL cells. (*b*) *In situ* hybridization for EBER of spleen from NOG mice not receiving tumor cells. as a negative control and tumor tissues of LCL cells injected mice. Magnification ×40. (*c*) Detection of viral DNA by PCR. M, Marker; U1: EBV-negative U937 cell for negative control; Ao1, *in vitro* culture and Ao2, Ao3 and Ao4, *in vivo* samples from 3 different mice inoculated with LCL-Ao; Ku1, *in vitro* culture and Ku2, Ku3 and Ku4, *in vivo* sample from 3 different mice inoculated with LCL-Ku; Ka1, *in vitro* culture and Ka2, Ka3 and Ka4, *in vivo* sample from 3 different mice inoculated with LCL-Ka, Ya1, *in vitro* culture and Ya2, Ya3 and Ya4, *in vivo* sample from 3 different mice inoculated with. LCL-Ya. Infiltration of EBV-immortalized B-cell lines in various organs of NOG mice. (*d*) HE and *in situ* hybridization for EBER of spleen, liver and lung of mice inoculated with LCL-Ku cells. Left, middle and right panels represent spleen, liver and lung, respectively. Upper and lower panels represent HE and EBER, respectively (magnification ×40).

Down-regulation of NF-κB occurred in all cell lines (Fig. 3*a*, upper panels). Inhibition appeared specific to NF-κB, because no significant change in binding activity of AP-1 was observed after treatment of cells with ritonavir (Fig. 3*a*, lower panels). Also, the observed protein/DNA binding was specific for NF-κB, because the binding was effectively competed and abrogated by excess unlabeled NF-κB oligonucleotide but not by mutant NF-κB or AP-1 oligonucleotide (Fig. 3*b*). LCL-Ku cell extract without ritonavir treatment contained p50, p65 and Rel B proteins in the NF-κB complex (Fig. 3*b*, upper panel), and ritonavir did not affect components of the NF-κB complex (Fig. 3*b*, lower panel).

Efficient engraftment and infiltration of EBV-transformed LCLs in NOG mice

EBV-immortalized LCLs (LCL-Ya, LCL-Ao, LCL-Ka and LCL-Ku) were inoculated s.c. in the post-auricular region of NOG mice (Fig. 4 and Table I). Mice inoculated with LCL cells (LCL-

TABLE I – *IN VIVO* CHARATERISTICS OF EBV-POSITIVE LYMPHOBLASTOID B CELLS IN NOG MICE

Cell line	Orgin/EBV status	No. of cells inoculated/mouse (10^7)[1]	Inoculation route[2]	Day of sacrifice after inoculation	No. of mice with tumor/no. of mice inoculated[3]	Organ-infiltration[4]		
						Spleen	Liver	Lung
LCL-Ya	B/+	1	sc	21	03/03	++	–	–
LCL-Ao	B/+	1	sc	21	03/03	++	–	–
LCL-Ka	B/+	1	sc	21	03/03	++	–	–
LCL-Ku	B/+	1	sc	21	21/21	+++	+	+

[1]Mice were inoculated with 1×10^7 cells per mouse.–[2]sc, subcutaneous.–[3]Number of animals in which tumor developed.–[4]Organ-infiltration was examined by histological analysis.–, no infiltration; +, slight infiltration; ++, marked infiltration; +++, massive infiltration.

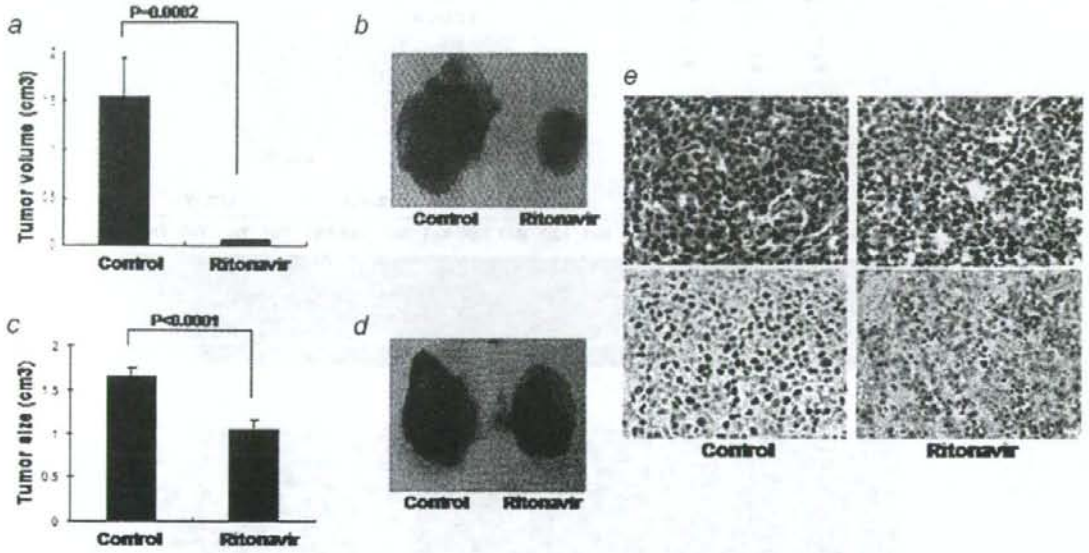

FIGURE 5 – Effect of ritonavir on lymphoma cell growth and infiltration. Mice were injected with LCL-Ku cells (1×10^7 cells) s.c. in the postauricular region. (*a* and *b*) The drug was administered s.c. into the tumor cells inoculated site of mice at doses of 30 mg/kg/day, beginning on day 0 for 3 weeks. The control mice received RPMI-1640 (200 µl) simultaneously. (*a*) Average size of tumor, data represent the mean ± SD from 6 mice. (*b*) Photograph of subcutaneously formed excised tumor without (left) and with (right) ritonavir treatment. (*c* and *d*) Effect of ritonavir on established tumor, ritonavir or RPMI-1640 was also administered intraperitoneally into mice as the same doses stated above, beginning on day 4 for 18 days. (*c*) Average size of tumor, data represent the mean ± SD from 6 mice. (*d*) Photograph of subcutaneously formed excised tumor without (left) and with (right) ritonavir treatment. (*e*) HE and *in situ* hybridization for EBER in spleen tissue of LCL cells injected mice. Magnification ×40. Upper and lower panels show HE and EBER staining, respectively.

Ya, LCL-Ao, LCL-Ka and LCL-Ku) produced a visible tumor within 3 weeks in all NOG mice. LCL-Ku cell was very efficient in the formation of a large tumor (Fig. 4*a*), as well as development of clinical signs of near-death, such as pilorection, weight loss and cachexia in mice at the time point of sacrifice. The average tumor size (LCL-Ya, LCL-Ao, LCL-Ka and LCL-Ku) in NOG mice inoculated s.c. with lymphoma cells was shown in Figure 4*a*. To test whether tumors maintain original histomorphology and expression patterns of tumor markers in NOG, we performed HE and *in situ* hybridization for EBER of normal mice spleen not receiving tumor cells and tumor tissues obtained from mice inoculated with LCLs. Histological analysis revealed that morphologically immunoblastic cells with large nucleus, clear nuclear membrane and broad cytoplasm expressed EBER, whereas EBER was not detected in spleen tissue collected from mice not receiving tumor cells, suggesting that *in vivo* tumor cells preserved well morphology as well as expressed viral gene EBER (Fig. 4*b*). Tumor cells from mice inoculated with EBV-immortalized B-cell lines were positive for DNA of EBV by PCR (Fig. 4*c*). These results showed that EBV-immortalized B-cell lines inoculated s.c. into the postauricular region of NOG mice were able to produce a visible tumor very efficiently. To assess the tissue distribution of lymphoma cells, we carried out histological examinations of the different organs of NOG mice after inoculation of the cells. Proliferation and infiltration of tumor cells were found not only in primary tumor tissues but also in spleen and to a lesser extent in liver and lung of NOG mice inoculated with tumor cells (Table I). HE and *in situ* hybridization staining for EBER showed a degree of infiltration of tumor cells at the site of inoculation and various organs with lymphoma cells (Fig. 4*d*). Interestingly, LCL-Ku cells appeared to infiltrate in various organs of mice more aggressively and massively than other cells. This extremely rapid tumor formation and infiltration in all mice is one of the hallmarks of our clinically relevant animal model without change of histomorphology or tumor marker expression.

Ritonavir suppresses the LCLs growth and infiltration in vivo

To determine the effect of ritonavir on tumor growth and infiltration, we injected LCL-Ku cells (1×10^7) s.c. into the postauricular region of NOG mice. Mice were treated with either RPMI-1640 (as control) or ritonavir (30 mg/kg/day), beginning on either day 0 or day 4. A significant decrease in the size of tumors in mice treated with ritonavir was demonstrated when compared with controls 3 weeks after the injection of tumor cells (Fig. 5*a*). Gross appearance of the mice treated by ritonavir showed apparent

reduction of the tumor mass at 3 weeks after inoculation of tumor cells (Fig. 5*b*). Ritonavir also inhibited the size and growth of established tumors (Fig. 5*c* and 5*d*). Ritonavir at this treatment dosage (30 mg/kg/day for 3 weeks) is well tolerated without adverse findings such as standing of hair, weight loss and cachexia of treated mice, all of which are signs of near death. Clinical evaluation of organ invasion 3 weeks after injection of tumor cells showed that ritonavir treatment inhibited their infiltration into spleen (Fig. 5*e*). In contrast, all control mice showed infiltration with tumor cells into spleen. Organ infiltration of lymphoma cells were analyzed and evaluated by HE and *in situ* hybridization of EBER. Together, these data indicate that ritonavir significantly inhibits lymphoma cell growth and infiltration in various organs of NOG mice (Fig. 5).These results suggest that ritonavir contributes to the reduction of the tumor growth and inhibits the organ infiltration in the mice through targeting the constitutive NF-κB activity.

Discussion

EBV-positive malignancies in immunocompromised patients are associated with high mortality and reduce overall survival period. The various chemotherapies so far developed have not increased significantly the survival of patients with EBV-associated malignancies in immunocompromised patients. Given disappointing results using conventional chemotherapy, new treatment strategies that specially target EBV-transformed cells are need.[1,2] LMP-1 is an oncogene that constitutively activates NF-κB to induce B cell proliferation.[7] It has been previously reported that suppression of high NF-κB activity inhibited cell growth and induced apoptosis of cancer cells as well as EBV-transformed cells both *in vitro* and *in vivo*.[12–20,33] Ritonavir is cytotoxic for different types of malignant cells *in vitro* through affecting proteasomal proteolysis, although concentrations necessary to show the *in vitro* effect exceed the achievable therapeutic drugs level.[27,29,30] It may affect the stabilization of p21. p27 and p53 proteins. Recently, ritonavir has been shown to inhibit NF-κB activity and induce the apoptosis of ATL cells.[20] This led us to investigate whether this drug exhibits anti-tumor effects against EBV-transformed cells *in vitro* and in our preclinical murine model. In the present study, we established a unique murine model that presents aggressive features concerning cell growth and infiltration in SCID mice within 3 weeks. Thus, it represents a novel model to evaluate tissue toxicity and the efficacy of therapeutic agents directed toward the treatment of EBV-associated lymphoproliferative diseases.

The blood-plasma ritonavir concentrations obtained in the therapy of HIV-infection are between 5 to 15 μM,[34] but much higher maximal concentrations (up to 46 μM) have been demonstrated in individual patients.[35] In the present study, we used the concentration of ritonavir for doing *in vitro* experiments from 0 to 40 μM and *in vivo* 30 mg/kg/day used for treatment of AIDS patients. Constitutive and strong NF-κB activation was reported to be a characteristic of LCL and important for LCL growth and survival.[7] Our results indicate that inhibition of NF-κB activity by ritonavir reduced cell growth and induced apoptosis of these cells. This is consistent with down-modulation of NF-κB regulated genes such as antiapoptotic and cell-cycle related genes. Our murine model clearly indicate that 30 mg/kg/day of ritonavir (the same dose used clinically for treating HIV/AIDS patients) significantly inhibits EBV-transformed cell growth and infiltration into various organs of NOG mice. The plasma exposure produced by this dose in mice is only approximately one-half of the plasma exposure observed with the licensed dose of ritonavir in human (600 mg BID). In our murine model, ritonavir at this treatment dosage is well tolerated without severe adverse effects observed in the mice during the treatment period. These data strongly suggest that the HIV protease inhibitor, ritonavir, is a promising antitumor agent against EBV-transformed cells and could be used clinically for treatment of EBV-associated malignancies. These results suggest that anti-tumor activity of ritonavir correlates with suppression of NF-κB activity.

In summary, we have established a novel NOG EBV-associated lymphoma model that presents features similar to patients with EBV-infection in immunocompromised patients. These results also indicate that the HIV protease inhibitor, ritonavir, showed antitumor and anti-NF-κB activity against EBV-transformed cells. Finally, our results strongly suggest that NF-κB serves as a potential molecular target to treat EBV-associated malignancies, and that ritonavir might be used clinically as a single compound or in combination with the reducing dose of chemotherapeutic agents for treatment of patients with life-threatening EBV-associated lymphoproliferative diseases and AIDS-associated lymphomas.

Acknowledgements

We thank D. Kempf and T. Yamada of Abbott Laboratories, S. Ichinose of Instrumental Analysis Research Center and S. Endo of Animal Research Center, Tokyo Medical and Dental University for their advice and assistance with the experiments. We also thank Y. Sato of the National Institute of Infectious Diseases for her excellent technical assistance.

References

1. Rickinson AB, Kieff E. Epstein-Barr virus. In: Fields BN, ed. Fields virology, 4th edn. New York (NY): Lippincott Williams and Wilkins, 2001. Vol. 1, 2575–627.
2. Kieff E, Rickinson AB. Epstein-Barr virus and replication. In: Fields BN, ed. Fields virology, 4th ed. New York (NY): Lippincott Williams and Wilkins, 2001. Vol. 1, 2511–73.
3. Zur Hausen H, Schulte-Holthausen H. Presence of EB virus nucleic acid homology in a "virus-free" line of Burkitt tumour cells. Nature 1970;227:245–48.
4. Nonoyama M, Pagano JS. Homology between Epstein-Barr virus DNA and viral DNA from Burkitt's lymphoma and nasopharyngeal carcinoma determined by DNA-DNA reassociation kinetics. Nature 1973;242:44–7.
5. Rowe M, Lear AL, Croom-Carter D, Davies AH, Rickinson AB. Three pathways of Epstein-Barr virus gene activation from EBNA1-positive latency in B lymphocytes. J Virol 1992;66:122–31.
6. Yamamoto N, Takizawa T, Iwanaga Y, Shimizu N, Yamamoto N. Malignant transformation of B lymphoma cell line BJAB by Epstein-Barr virus-encoded small RNAs. FEBS Lett 2000;484:153–58.
7. Mosialos G, Birkenbach M, Yalamanchili R, VanArsdale T, Ware C, Kieff E. The Epstein-Barr virus transforming protein LMP1 engages signaling proteins for the tumor necrosis factor receptor family. Cell 1995;80:389–99.
8. Mori N, Fujii M, Ikeda S, Yamada Y, Tomonaga M, Ballard DW, Yamamoto N. Constitutive activation of NF-κB in primary adult T-cell leukemia cells. Blood 1999;93:2360–8.
9. Baldwin AS. The NF-κB and IκB proteins: new discoveries and insights. Annu Rev Immunol 1999;14:649–81.
10. Guinness ME, Kenney JL, Reiss M, Lacy J. Bcl-2 antisense oligodeoxynucleotide therapy of Epstein-Barr virus-associated lymphoproliferative disease in severe combined immunodeficient mice. Cancer Res 2000;60:5354–8.
11. Miyake A, Dewan MZ, Ishida T, Watanabe M, Honda M, Sata T, Yamamoto N, Umezawa K, Watanabe T, Horie R. Induction of apoptosis in Epstein-Barr virus-infected B-lymphocytes by the NF-kappaB inhibitor DHMEQ. Microbes Infect 2008;10:748–56.
12. Watanabe M, Dewan MZ, Okamura T, Sasaki M, Itoh K, Higashihara M, Mizoguchi H, Honda M, Sata T, Watanabe T, Yamamoto N, Umezawa K, et al. A novel NF-κB inhibitor DHMEQ selectively targets constitutive NF-κB activity and induces apoptosis of multiple myeloma cells in vitro and in vivo. Int J Cancer 2005;114:32–8.
13. Adams J, Palombella VJ, Elliott PJ. Proteasome inhibition: a new strategy in cancer treatment. Invest New Drugs 2001;18:109–21.
14. Teicher BA, Ara G, Herbst R, Palombella VJ, Adams J. The proteasome inhibitor PS-341 in cancer therapy. Clin Cancer Res 1999; 5:2638–45.

15. Hideshima T, Chauhan D, Richardson P, Mitsiades C, Mitsiades N, Hayashi T, Munshi N, Dang L, Castro A, Palombella V, Adams J, Anderson KC. NF-κB as a therapeutic target in multiple myeloma. J Biol Chem 2002;277:16639–47.
16. Dewan MZ, Terashima K, Taruishi M, Hasegawa H, Ito M, Tanaka Y, Mori N, Sata T, Koyanagi Y, Maeda M, Kubuki Y, Okayama A, et al. Rapid tumor formation of human T-cell leukemia virus type 1-infected cell lines in novel NOD-SCID/γc^{null} mice: suppression by an inhibitor against NF-κB. J Virol 2003;77:5286–94.
17. Kitajima I, Shinohara T, Bilakovics J, Brown DA, Xu X, Nerenberg M. Ablation of transplanted HTLV-I Tax-transformed tumors in mice by antisense inhibition of NF-κB. Science 1992;258:1792–5.
18. Mori N, Yamada Y, Ikeda S, Yamasaki Y, Tsukasaki K, Tanaka Y, Tomonaga M, Yamamoto N, Fujii M. Bay 11–7082 inhibits transcription factor NF-κB and induces apoptosis of HTLV-I-infected T-cell lines and primary adult T-cell leukemia cells. Blood 2002;100:1828–34.
19. Tan C, Waldmann TA. Proteasome inhibitor PS-341, a potential therapeutic agent for adult T-cell leukemia. Cancer Res 2002;62: 1083–6.
20. Dewan MZ, Uchihara JN, Terashima K, Honda M, Sata T, Ito M, Fujii N, Uozumi K, Tsukasaki K, Tomonaga M, Kubuki Y, Okayama A, et al. Efficient intervention of growth and infiltration of primary adult T-cell leukemia cells by an HIV protease inhibitor, ritonavir. Blood 2006;107:716–24.
21. Cahir-McFarland ED, Davidso DM, Schauer SL, Duong J, Kieff E. NF-kappa B inhibition causes spontaneous apoptosis in Epstein-Barr virus-transformed lymphoblastoid cells. Proc Natl Acad Sci USA 2000;97:6055–60.
22. Collier AC. Efficacy of combination antiretroviral therapy. Adv Exp Med Biol 1996;394:355–72.
23. Collier AC, Coombs RW, Schoenfeld DA, Bassett R, Baruch A, Corey L. Combination therapy with zidovudine, didanosine and saquinavir. Antiviral Res 1996;29:99.
24. Collier AC, Coombs RW, Schoenfeld DA, Bassett RL, Timpone J, Baruch A, Jones M, Facey K, Whitacre C, McAuliffe VJ, Friedman HM, Merigan TC, et al. Treatment of human immunodeficiency virus infection with saquinavir, zidovudine, and zalcitabine. AIDS Clinical Trials Group. N Engl J Med 1996;334:1011–17.
25. Markowitz M, Saag M, Powderly WG, Hurley AM, Hsu A, Valdes JM, Henry D, Sattler F, La Marca A, Leonard JM, Ho DD. A preliminary study of ritonavir, an inhibitor of HIV-1 protease, to treat HIV-1 infection. N Engl J Med 1995;333:1534–39.
26. Kempf DJ, Marsh KC, Denissen JF, McDonald E, Vasavanonda S, Flentge CA, Green BE, Fino L, Park CH, Kong XP, Wideburg NE, Saldivar A, et al. ABT-538 is a potent inhibitor of human immunodeficiency virus protease and has high oral bioavailability in humans. Proc Natl Acad Sci USA 1995;92:2484–88.
27. Andre P, Groettrup M, Klenerman P, de Giuli R, Booth BL, Jr, Cerundolo V, Bonneville M, Jotereau F, Zinkernagel RM, Lotteau V. An inhibitor of HIV-1 protease modulates proteasome activity, antigen presentation, and T cell responses. Proc Natl Acad Sci USA 1998; 95:13120–24.
28. Liang JS, Distler O, Cooper DA, Jamil H, Deckelbaum RJ, Ginsberg HN, Sturley SL. HIV protease inhibitors protect apolipoprotein B from degradation by the proteasome: a potential mechanism for protease inhibitor-induced hyperlipidemia. Nat Med 2001;7:1327–31.
29. Schmidtke G, Holzhütter HG, Bogyo M, Kairies N, Groll M, de Giuli R, Emch S, Groettrup M. How an inhibitor of the HIV-I protease modulates proteasome activity. J Biol Chem 1999;274:35734–40.
30. Gaedicke S, Firat-Geier E, Constantiniu O, Lucchiari-Hartz M, Freudenberg M, Galanos C, Niedermann G. Antitumor effect of the human immunodeficiency virus protease inhibitor ritonavir: induction of tumor-cell apoptosis associated with perturbation of proteasomal proteolysis. Cancer Res 2002;62:6901–8.
31. Pati S, Pelser CB, Dufraine J, Bryant JL, Reitz JMS, Weichold FF. Antitumorigenic effects of HIV protease inhibitor ritonavir: inhibition of Kaposi sarcoma. Blood 2002;99:3771–9.
32. Sgadari C, Barillari G, Toschi E, Carlei D, Bacigalupo I, Baccarini S, Palladino C, Leone P, Bugarini R, Malavasi L, Cafaro A, Falchi M, et al. HIV protease inhibitors are potent anti-angiogenic molecules and promote regression of Kaposi sarcoma. Nat Med 2002;8:225–32.
33. Katano H, Pesnicak H, Cohen JI. Simvastatin induces apoptosis of Epstein-Barr virus (EBV)-transformed lymphoblastoid cell lines and delays development of EBV lymphomas. Proc Natl Acad Sci USA 2004;101:4960–5.
34. Norvir, Ritonavir Product monograph. North Chicago, IL: Abbott laboratories, 1997.
35. Gatti G, Di Biagio A, Casazza R, De Pascalis C, Bassetti M, Cruciani M, Vella S, Bassetti D. The relationship between ritonavir plasma levels and side-effects: implications for therapeutic drug monitoring. AIDS 1999;13:2083–9.

研究成果の刊行に関する一覧表
平成 20 年度　慶應義塾大学医学部　熱帯医学・寄生虫学教室　竹内　勤

雑誌

発表者氏名	論文タイトル名	発表誌名	巻号	ページ	出版年
Takuya Maeda, Tomoya Saito, Omar S. Harb, David S. Roos, Satoru Takeo, Hiroko Suzuki, Takafumi Tsuboi, Tsutomu Takeuchi, Takashi Asai	Pyruvate Kinase type-II isozyme in Plasmodium falciparum localizes to the apicoplast	Parasitology International	58	101-105	2009
Jun Suzuki, Seiki Kobayashi, Ph.D., Rie Murata, Hideo Tajima, D.V.M., Fumitaka Hashizaki, D.V.M., Yoshitoki Yanagawa, D.V.M., Ph.D., Tsutomu Takeuchi, M.D., Ph.D.	A SURVEY OF AMOEBIC INFECTIONS AND DIFFERENTIATION OF AN ENTAMOEBA HISTOLYTICA-LIKE VARIANT(JSK2004) IN NONHUMAN PRIMATES BY A MULTIPLEX POLYMERASE CHAIN REACTION	Journal of Zoo and Wildlife Medicine	39	370-379	2008
Masashi Ohtani, Shigenori Nagai, Shuhei Kondo, Shinta Mizuno, Kozue Nakamura, Masanobu Tanabe, Tsutomu Takeuchi, Satoshi Matsuda, Shigeo Koyasu	Mammalian target of rapamycin and glycogen synthase kinase 3 differentially regulate lipopolysaccharide-induced interleukin-12 production in dendritic cells	IMMUNO-BIOLOGY	112	635-643	2008
Tomoya Saito, Manami Nishi, Muoy l. Lim, Bo Wu, Takuya Maeda, Hisayuki Hashimoto, Tsutomu Takeuchi, David S. Roos, Takashi Asai	A Novel GDP-dependent Pyruvate Kinase Isozyme from Toxoplasma gondii Localizes to Both the Apicoplast and the Mitochondrion	THE JOURNAL OF BIOLOGICAL CHEMISTRY	283	14041-14052	2008
Jun Suzuki, Seiki Kobayashi, Ise Iku, Rie Murata, Yoshitoki Yanagawa and Tsutomu Takeuchi	Seroprevalence of Entamoeba histolytica Infection in Female Outpatients at a Sexually Transmitted Disease Sentinel Clinic in Tokyo, Japan	Jpn. J. Infect. Dis.	61	175-178	2008
Kazutomo Suzue, Seiki Kobayashi, Tsutomu Takeuchi, Mamoru Suzuki Shigeo Koyasu	Critical role of dendritic cells in determining the T_h1/T_h2 balance upon Leishmania major infection	International Immunology	20	337-343	2008

Parasitology International 58 (2009) 101–105

Contents lists available at ScienceDirect

Parasitology International

journal homepage: www.elsevier.com/locate/parint

Short communication

Pyruvate kinase type-II isozyme in *Plasmodium falciparum* localizes to the apicoplast

Takuya Maeda [a,1], Tomoya Saito [a], Omar S. Harb [b], David S. Roos [b], Satoru Takeo [c], Hiroko Suzuki [c], Takafumi Tsuboi [c], Tsutomu Takeuchi [a], Takashi Asai [a,*]

[a] Department of Tropical Medicine and Parasitology, School of Medicine, Keio University, 35 Shinanomachi, Shinjuku-ku, Tokyo 160-8582, Japan
[b] Department of Biology, University of Pennsylvania, 301 Goddard Laboratories Philadelphia, PA 19104, USA
[c] Cell-Free Science and Technology Research Center, Ehime University, 3 Bunkyo-cho, Matsuyama, Ehime 790-8577, Japan

ARTICLE INFO

Article history:
Received 16 July 2008
Received in revised form 15 October 2008
Accepted 18 October 2008
Available online 31 October 2008

Keywords:
Plasmodium falciparum
Pyruvate kinase II
Apicoplast
Mitochondria
Cell-free expression

ABSTRACT

Bioinformatics research on *Plasmodium falciparum* revealed two isoforms of pyruvate kinase: type-I and type-II enzymes. The type-I enzyme shows typical glycolytic properties, while type-II enzyme is involved in fatty acid type-II biosynthesis and has been predicted to localize to the apicoplast with the targeting signal in its N-terminus. The type-I and type-II isoforms have the same evolutionary origin as *Toxoplasma gondii* isozymes, *Tg*PyKI and *Tg*PyKII, respectively; however, *Tg*PyKII localizes to both the mitochondrion and the apicoplast. Accordingly, we made a recombinant full length of *P. falciparum* pyruvate kinase type-II protein using a wheat germ cell-free expression system and obtained a specific antibody against the type-II protein. Fluorescent microscopic analysis revealed that *P. falciparum* type-II enzyme was localized only to the apicoplast, not to the mitochondrion. The data suggest differences in localization and metabolic pathways between *P. falciparum* and *T. gondii* pyruvate kinase isoforms.

Pyruvate kinase (EC 2.7.1.40) catalyzes the essentially irreversible transphosphorylation of phosphoenolpyruvate (PEP) to ADP. The activities of most mammalian and bacterial pyruvate kinases are allosterically regulated by fructose 1,6-bisphosphate, and pyruvate kinase is known to play a regulatory role in glycolysis. The glycolytic end product, pyruvate, feeds into various metabolic pathways, and hence pyruvate kinase is important in several primary metabolic reactions.

Many organisms have pyruvate kinase isozymes with different kinetic properties, and most pyruvate kinases in eukaryotes are reported to be located in the cytosol. Two types of pyruvate kinase were characterized in *Toxoplasma gondii* [1,2]. Pyruvate kinase type-II isozyme (*Tg*PyKII) was localized in both the mitochondrion and the apicoplast, whereas pyruvate kinase type-I (*Tg*PyKI) was located in the cytosol. *Tg*PyKII exhibited only 18% overall amino acid identity with *Tg*PyKI and showed novel properties of exhibiting high pH optima and GDP dependency [2].

The malaria bioinformatics website (http://sites.huji.ac.il/malaria/), compiled and maintained by Hagai Ginsburg, reports two isoforms of pyruvate kinase in *Plasmodium falciparum*. The type-I enzyme (*Pf*PyKI) has been characterized enzymologically in detail [3]. The type-II enzyme (*Pf*PyKII) was predicted to have an apicoplast targeting signal in the N-terminus; however, experimental localization has not been confirmed. Phylogenetic analysis indicated that *Pf*PyKI and *Pf*PyKII have the same evolutionary origin as *Tg*PyKI and *Tg*PyKII, respectively, suggesting that type-II has a proteobacterial origin [2]. Thus, we questioned whether both *Pf*PyKII and *Tg*PyKII are localized in both the apicoplasts and the mitochondria.

In this study, we made recombinant *Pf*PyKII protein in a wheat germ cell-free expression system, purified the recombinant protein, created an antibody, and localized *Pf*PyKII by immunofluorescent microscopy.

The *Pf*PyKII gene was amplified from *P. falciparum* genomic DNA. The two primers were 5′-ACTGGATCCCCATATTGCCTATGAT-3′ and 5′-TCGGGATCC CTAATTTGTTAGACATGG-3′ (*Bam*HI site is underlined). The first denaturation at 95 °C was for 10 min and each of 30 reaction cycles consisted of 94 °C for 30 s, 47 °C for 30 s, and 65 °C for 2 min, and a final elongation cycle step at 65 °C for 5 min using KOD-plus DNA polymerase (Toyobo Co. Ltd, Osaka, Japan). Thereafter, the amplified DNA products were treated with *Bam*HI and inserted into a plasmid pEU-E01G-N2 (Cell-Free Science and Technology Research Center, Ehime University, Ehime, Japan) using the LigaFast ligation kit (Promega, Madison, WI, USA) according to the manufacturer's protocol. The plasmid was electroporated into the *Escherichia coli* DH10B (Takara Bio, Kyoto, Japan) and the bacteria were grown in a plate. The right directional clones were detected by DNA sequencing using the ABI PRISM BigDye terminator cycle sequencing kit (Applied Biosystems, Foster, CA, USA) and loaded onto an ABI PRISM 310 DNA sequencer. After plasmid purification

* Corresponding author. Tel.: +81 3 3353 1211x62747; fax: +81 3 3353 5958.
E-mail address: asait@sc.itc.keio.ac.jp (T. Asai).
[1] Present address: International Research Center for Infectious Diseases, The Institute of Medical Science, The University of Tokyo, Shiroganedai 4-6-1, Minato-ku, Tokyo 108-8639, Japan.

1383-5769/$ – see front matter © 2008 Elsevier Ireland Ltd. All rights reserved.
doi:10.1016/j.parint.2008.10.005

using Qiagen Plasmid Midi Kit (Qiagen, Hilden, Germany), the plasmid was further purified by $CsCl_2$ ultra-centrifugation at 391,000 ×*g* for 16 h at 25 °C to avoid endotoxin contamination. The purified plasmid containing a glutathione S-transferase (GST) coding region and an SP6 promoter upstream of the DNA inserted region was treated with SP6 RNA polymerase (GE Healthcare, Little Chalfont, Buckinghamshire, UK). The method of mRNA production and translation in wheat germ was described previously [4].

The GST-pyruvate kinase isozyme fusion protein in the wheat germ extract was purified using an affinity column of glutathione sepharose 4B (GE Healthcare). The pyruvate kinase isozyme was cut from the fusion protein by PreScission Protease (GE Healthcare) according to

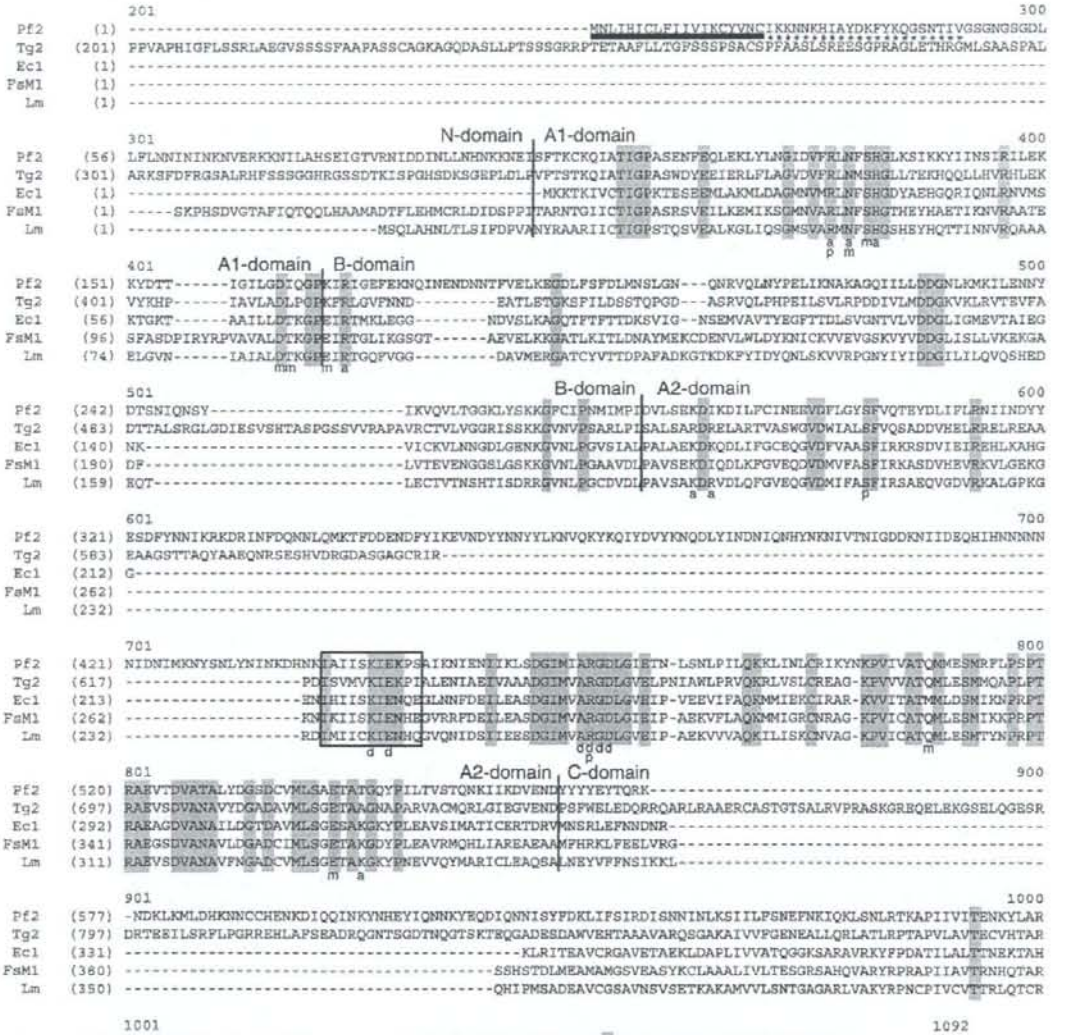

Fig. 1. Amino acid sequence alignment of *P. falciparum* pyruvate kinase type-II isozyme (*Pf*PyKII) with four pyruvate kinases from other species. Sequence data accession numbers are: Pf2, *Pf*PyKII (this study; PF10_0363); Tg2, *Toxoplasma gondii* II (AB118155); Ec1, *Escherichia coli* isozyme I (1PKY_A); FsM1, *Felis catus* isozyme M1 (P11979); Lm, *Leishmania mexicana* (CAA52898). *Vertical lines* indicate divisions between four three-dimensional domains (N, A, B, and C) as described previously [10]. An open black *box* indicates the pyruvate kinase signature sequence (PROSITE, PS00110); *p* indicates PEP binding sites; *a*, ADP binding sites; *d*, divalent cation binding sites; *m*, monovalent cation binding sites; *dashes*, gaps in the alignment. DNA sequences analyses were performed using the VectorNTI suite (InforMax, Executive Way Frederick, MD, USA). The thick underline in the N-terminal of *P. falciparum* sequence is signal sequence, and following asterisks indicates probable plastid transit peptide. It is conceivable that these sequences compose apicoplast targeting signal. Targeting signals in the N-terminal were analyzed by SignalP [11] and PlasmoAP [12].

the manufacturer's recommendations. Pyruvate kinase isozyme purity was analyzed by SDS–PAGE on 8% polyacrylamide gel as described by Laemmli [5] (Data not shown). The recombinant protein concentration was determined by Bradford assay [6] using bovine serum albumin (BSA) as a standard.

Anti-recombinant *Pf*PyKII antibody was produced through a commercial company (Immuno-Biological Laboratories, Takasaki, Japan). Briefly, purified recombinant *Pf*PyKII from wheat germ extracts was used to immunize a BALB/c mouse. Following six injections of pyruvate kinase isozyme (5 μg each) at 1-week intervals, the whole IgG was isolated from peritoneal fluid with a HiTrap rProtein A FF column (GE Healthcare). The whole cell lysate of 1×10^8 erythrocytic stage *P. falciparum* parasites (FCR-3 strain) was separated on 8% acrylamide gel and blotted onto a nitrocellulose Hybond-C Extra membrane (GE Healthcare). The membrane was blocked for 20 min with 2% skimmed milk in Tris-buffered saline containing 0.2% Tween 20, incubated for 1 h with primary antibodies (1:3000), probed with alkaline phosphatase-conjugated goat anti-mouse IgG (Vector Laboratories, Burlingame, CA, USA) (1:5000), and detected with a BCIP-NBT system (Roche, Basel, Switzerland). Molecular sizes of the protein bands were determined with reference to pre-stained Rainbow molecular weight markers (GE Healthcare).

Cells were fixed and stained using the procedures described by Tonkin et al. [7]. Cells were briefly fixed with 4% EM grade paraformaldehyde (ProSciTech, Thuringowa, Queensland, Australia) and 0.0075% EM grade glutaraldehyde (ProSciTech) in phosphate-buffered saline (PBS) for 30 min. Fixed cells were washed once in PBS and permeated with 0.1% Triton X-100/PBS for 10 min. Cells were washed again and treated with 0.1 mg/ml of sodium borohydride ($NaBH_4$)/PBS for 10 min. Following another wash, cells were blocked in 3% BSA/PBS for 1 h. For staining anti-*Pf*PyKII antibody-binding structure and apicoplast, anti-*Pf*PyKII mouse antibody (diluted 1/1000) and anti-acyl carrier protein (ACP) rabbit antibody (diluted 1/500; gifted by Geoff McFadden, University of Melbourne, Australia) were added and allowed to bind for a minimum of 1 h in 3% BSA/PBS. AlexaFluor goat anti-mouse 594 (red) and anti-rabbit 488 (green) secondary antibodies (Invitrogen, Carlsbad, CA, USA) were added at 1:1000 dilution (in 3% BSA/PBS) and allowed to bind for 1 h, while cells settled onto a previously flamed cover slip coated with 1% polyethylenimine (PEI; Sigma, St Louis, MO, USA). For staining the anti-*Pf*PyKII antibody-binding structure and mitochondrion, citrate synthase-GFP construct (gifted by Geoff McFadden) transformed *P. falciparum* was used. Anti-*Pf*PyKII mouse antibody (diluted 1/1000) was added and allowed to bind for 1 h, followed by addition of AlexaFluor goat anti-mouse 488 (green) antibody and Cy5-conjugated anti-GFP rabbit (red) antibody (diluted 1/1000; Sigma) and allowed to bind for 1 h. Cells were mounted in 50% glycerol with 0.1 mg/ml of 1,4-diazabicyclo[2.2.2]octane (DABCO, Sigma). The microscopic system was a DeltaVision restoration system (Applied Precision, Washington, USA) on an Olympus IX70 inverted microscope equipped with a mercury vapor lamp (100 W) and appropriate barrier emission filters. Images were taken 0.2 μm apart and deconvolved using softWoRx Explorer Suite (Applied Precision).

The deduced amino acid sequence of *Pf*PyKII (NCBI Accession# NP_700836), exhibiting low overall identity (21%) to that of *Pf*PyKI (NCBI Accession# CAG25081), contained a pyruvate kinase signature (PROSITE; PS00110) as did other species and other consensus regions, such as multiple binding sites of ADP, PEP, and divalent cations (Fig. 1). Based on protein alignment, *Pf*PyKII was predicted to be a monovalent cation-independent enzyme. Most of the monovalent cation-binding sites were conserved; however, two binding sites, Thr^{113} and Glu^{117} (in *Felis catus* pyruvate kinase), were substituted by Ile and Lys, respectively. These substitutions are a common characteristic of monovalent cation-independent pyruvate kinases. We found three-specific long insertions in the middle of domain B, A2, and C of *Pf*PyKII, as in *Tg*PyKII. These insertions were different in length, but the insert positions were the same as in *Tg*PyKII.

Following six injections of pyruvate kinase isozyme at 1-week intervals, the whole IgG was isolated from mouse peritoneal fluid. Western blot analysis showed a single band (~80 kDa) in the *P. falciparum* lysate (Fig. 2), which was different from the mass in the type-I enzyme (55.6 kDa), indicating no cross-reaction with the type-I enzyme. Preimmune serum detected no bands in the 1×10^8 *P. falciparum* lysate (data not shown). The antibody was used in immunofluorescence microscopy.

The stained structure from the anti-*Pf*PyKII antibody in *P. falciparum* merged into the apicoplast stained pattern (Fig. 3A), suggesting that *Pf*PyKII localizes to the apicoplast. To determine if *Pf*PyKII localizes to the mitochondria, we analysed the immunolocalization of *Pf*PyKII in a *P. falciparum* cell line expressing the citrate synthase fused to GFP, which targets to the mitochondria [7] (Fig. 3B). The merged image showed that anti-*Pf*PyKII stain is adjacent to, but not associated with, the mitochondria. The two stains were distinguishable in all the stages (data not shown). Thus, we concluded that *Pf*PyKII localizes to the apicoplast, not to the mitochondrion. The data indicate a different localization of type-II pyruvate kinase in *P. falciparum* from that in *T. gondii*.

A recombinant protein of *P. falciparum* pyruvate kinase type-II isozyme (*Pf*PyKII) was created using a wheat germ cell-free system. All our previous attempts for production of this recombinant protein in *E. coli* systems have failed. Probably, it was due to its biased codon usage. The efficiency of production of the protein in our study was not high; nevertheless, the wheat germ cell-free system is useful for creation of the recombinant protein.

In addition, we showed localization of *Pf*PyKII in the apicoplast by immunofluorescent assay. Despite its proteobacterial origin, *Pf*PyKII was localized only to the apicoplast, not to the mitochondrion as in *Tg*PyKII, which is localized to both the mitochondrion and the apicoplast. The difference in metabolic pathways in the organelles between *T. gondii* and *P. falciparum* might reflect differences in their internal environment and in the metabolic relationships between those organelles in the two parasites. Further investigation to reveal these potential differences will contribute to understanding survival of *T. gondii* and *P. falciparum* in the host.

As suggested by Ralph et al. [8], pyruvate kinase in the apicoplast might dephosphorylate PEP imported into the apicoplast via PEP transporter on the apicoplast membrane and supply pyruvate for fatty acid synthesis and the non-mevalonate 1-deoxy-D-xylulose-5-phophate (DOXP) pathway in the organelle. Fleige et al. [9], reporting on carbohydrate metabolism in the *T. gondii* apicoplast, indicated that *Tg*PykII was localized in the apicoplast. These findings suggest differences between *T. gondii* and *P. falciparum* in the mitochondrion and apicoplast metabolic pathways, even though *T. gondii*

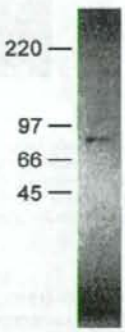

Fig. 2. Specificity of anti-*Pf*PyKII IgG shown by Western blot analysis. The purified recombinant *Pf*PyKII was detected by Western blot analysis with the antibody against the recombinant *Pf*PyKII. Rainbow molecular weight markers (kDa) are indicated on the left.

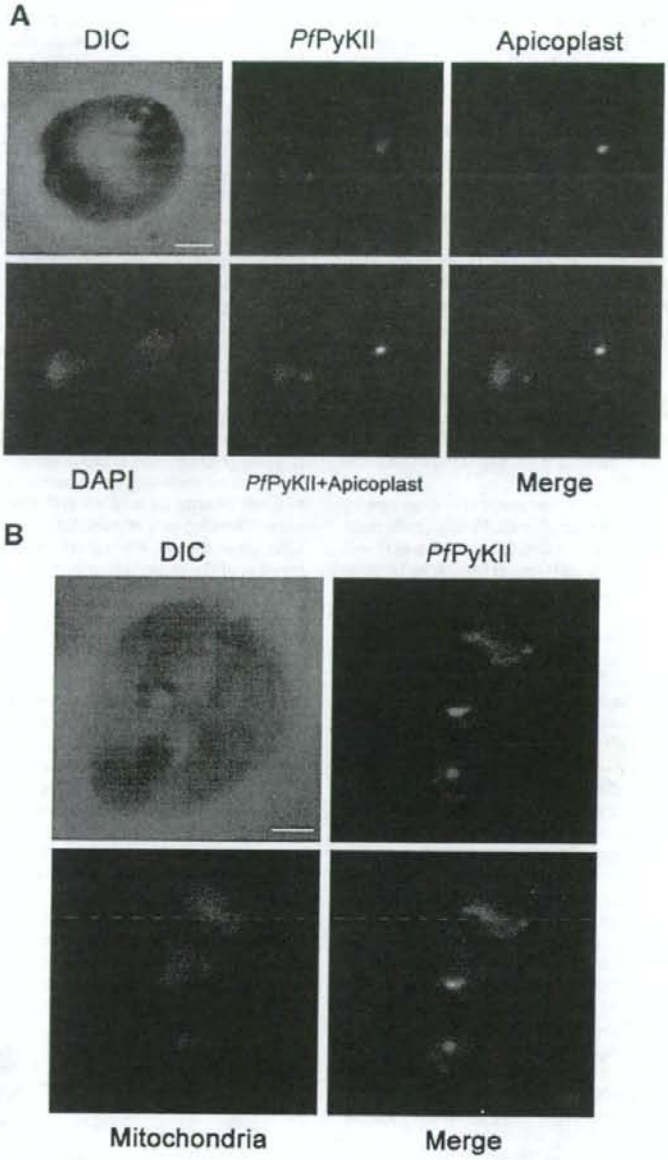

Fig. 3. Immunofluorescent microscopic analysis of co-localization of *Pf*PyKII with the apicoplast, but not with the mitochondrion in red blood cells infected with *P. falciparum*. A: Anti-*Pf*PyKII and anti-*P. falciparum* ACP antibodies detected by AlexaFlour goat anti-mouse 594 (red) and goat anti-rabbit 488 (green) secondary antibodies, respectively. Immunofluoresecnce of *P. falciparum* ACP antibody shows the apicoplast. Merged images indicate co-localization of *Pf*PyKII and *P. falciparum* ACP. Nucleus stained by DAPI (blue). B: Red blood cells infected with parasites expressing citrate synthase fused to GFP targeting the mitochondrion (Tonkin et al. 2004). GFP detected by Cy5-conjugated goat anti-GFP (red). Anti-*Pf*PyKII antibody detected by AlexaFluor goat anti-mouse 488 (green) IgG. Merged image shows that *Pf*PyKII does not co-locate with the mitochondrion. White scale bars are 2 μm.

and *P. falciparum* have comparable organelle components, and were thought to have similar enzyme components in both the apicoplast and the mitochondrion. The pathway differences might reflect differences in intracellular environments or different abilities to import metabolites into those organelles. We expected that the difference in enzymatic properties between *Tg*PyKII and *Pf*PyKII would help in understanding their roles in the two parasites, but several attempts to express the active recombinant enzyme have failed. As pyruvate kinase has been thought to play a role only in glycolysis in the cytosol, pyruvate kinases localized with cell organelles are unique. Non-glycolytic pyruvate kinases have been found only in the apicomplexan parasites, such as *Plasmodium* sp,

Theileria sp, and *T. gondii*. Characterization of non-glycolytic pyruvate kinases would increase the understanding of the unique metabolic pathways in protozoan parasites.

In addition to uncertainty about metabolic pathways, we are also uncertain about the origin of *Pf*PyKII. Although *Pf*PyKII exhibits a typical bipartite signal in the N-terminus, *Pf*PyKII has a proteobacterial origin, which is indicative of the apicoplast protein, and not a cyanobacterial or plastidic origin [2]. We suggest that *Pf*PyKII might have been obtained from endosymbiotic bacteria. Originally *Pf*PyKII may have localized in both the mitochondrion and the apicoplast, as in *T. gondii*; subsequently *P. falciparum* may have lost the mitochondrial location during evolutionary development.

Acknowledgements

We thank Dr. Shinichiro Kawazu (Obihiro University of Agriculture and Veterinary Medical) for providing genomic DNA of *P. falciparum*, and Dr. Geoffrey I. McFadde (University of Melbourne) for providing both anti-acyl carrier protein rabbit antibody and *P. falciparum* expressing citrate synthase fused to GFP. This work was supported in part by Keio Gijuku Academic Development Funds, Japan.

References

[1] Maeda T, Saito T, Oguchi Y, Nakazawa M, Takeuchi T, Asai T. Expression and characterization of recombinant pyruvate kinase from *Toxoplasma gondii* tachyzoites. Parasitol Res 2003;89:259–65.
[2] Saito T, Nishi M, Lim MI, Wu B, Maeda T, Hashimoto H, Takeuchi T, Roos DS, Asai T. A novel GDP-dependent pyruvate kinase isozyme from *Toxoplasma gondii* localizes to both the apicoplast and the mitochondrion. J Biol Chem 2008;283:14041–52.
[3] Chan M, Sim TS. Functional analysis, overexpression, and kinetic characterization of pyruvate kinase from *Plasmodium falciparum*. Biochem Biophys Res Commun 2004;326:188–96.
[4] Sawasaki T, Gouda MD, Kawasaki T, Tsuboi T, Tozawa Y, Takai K, Endo Y. The wheat germ cell-free expression system: methods for high-throughput materialization of genetic information. Methods Mol Biol 2005;310:131–44.
[5] Laemmli UK. Cleavage of structural proteins during the assembly of the head of bacteriophage T4. Nature 1970;227:680–5.
[6] Bradford MM. A rapid and sensitive method for the quantitation of microgram quantities of protein utilizing the principle of protein-dye binding. Anal Biochem 1979;72:248–54.
[7] Tonkin CJ, van Dooren GG, Spurck TP, Struck NS, Good RT, Handman E, Cowman AF, McFadden GI. Localization of organellar proteins in *Plasmodium falciparum* using a novel set of transfection vectors and a new immunofluorescence fixation method. Mol Biochem Parasitol 2004;137:13–21.
[8] Ralph SA, van Dooren GG, Waller RF, Crawford MJ, Fraunholz MJ, Foth BJ, Tonkin CJ, Roos DS, McFadden GI. Tropical infectious diseases: metabolic maps and functions of the *Plasmodium falciparum* apicoplast. Nat Rev Microbiol 2004;2:203–16.
[9] Fleige T, Fischer K, Ferguson DJP, Gross U, Bohne W. Carbohydrate metabolism in the *Toxoplasma gondii* apicoplast: localization of three glycolytic isoenzymes, the single pyruvate dehydrogenase complex, and a plastid phosphate translocator. Eukaryot Cell 2007;6:984–96.
[10] Rigden DJ, Phillips SE, Michels PA, Fothergill-Gilmore LA. The structure of pyruvate kinase form *Leishmania mexicana* reveals details of the allosteric transition and unusual effector specificity. J Mol Biol 1999;291:615–35.
[11] Bendtsen JD, Nielsen H, von Heijne G, Brunak S. Improved prediction of signal peptides: SignalP 3.0. J Mol Biol 2004;340:783–95.
[12] Foth BJ, Ralph SA, Tonkin CJ, Struck NS, Fraunholz M, Roos DS, Cowman AF, McFadden GI. Dissecting apicoplast targeting in the malaria parasite *Plasmodium falciparum*. Science 2003;299(5607):705–8.

Journal of Zoo and Wildlife Medicine 39(3): 370–379, 2008

A SURVEY OF AMOEBIC INFECTIONS AND DIFFERENTIATION OF AN *ENTAMOEBA HISTOLYTICA*–LIKE VARIANT (JSK2004) IN NONHUMAN PRIMATES BY A MULTIPLEX POLYMERASE CHAIN REACTION

Jun Suzuki, Seiki Kobayashi, Ph.D., Rie Murata, Hideo Tajima, D.V.M., Fumitaka Hashizaki, D.V.M., Yoshitoki Yanagawa, D.V.M., Ph.D., and Tsutomu Takeuchi, M.D., Ph.D.

Abstract: A pathogenic *Entamoeba histolytica*–like variant (JSK2004 strain) with genetic variations and a novel isoenzyme pattern isolated from a De Brazza's guenon in a Tokyo zoo in Japan has previously been documented. In this study, a multiplex polymerase chain reaction (PCR) assay that could distinguish the JSK2004-type *E. histolytica*–like variant (JSK04-Eh-V) from *E. histolytica* and *Entamoeba dispar* using three newly designed primer sets for amplifying each specific DNA fragment from their small-subunit ribosomal RNA genes was developed and established. Forty-seven primates (11 species) from the zoo were surveyed by multiplex PCR to assess the prevalence of JSK04-Eh-V infection, which was recognized in six individuals of four species, including an Abyssinian colobus monkey, a De Brazza's guenon (including the individual from whom JSK2004 was isolated), a white-faced saki, and a Geoffroy's spider monkey. In addition, the autopsied individuals of an Abyssinian colobus and Geoffroy's spider monkey that died of amoebic liver abscess were also evaluated. DNA samples were also analyzed for specific genotypes based on the nucleotide sequencing of two protein-coding (chitinase and serine-rich *E. histolytica* protein) genes and the protein-noncoding locus 1-2 that was used for fingerprinting of the *E. histolytica* strain. These studies indicated that the *E. histolytica*–like variant infection in this zoo was caused by the same type (i.e., JSK04-Eh-V). An axenic culture medium (yeast extract–iron–maltose–dihydroxyacetone–serum) was developed based on the yeast extract–iron–gluconic acid–dihydroxyacetone–serum medium, which is designed for axenic culture of *E. dispar*. This new medium could be used for axenically culturing *E. histolytica*, JSK04-Eh-V, and *E. dispar* in a single medium.

Key words: *Entamoeba histolytica*–like variant, multiplex PCR, nonhuman primates, zoo.

INTRODUCTION

Amoebiasis is a zoonotic protozoal infectious disease caused by *Entamoeba histolytica*. The estimated incidence of amoebiasis in humans is approximately 50 million per year, and it has caused nearly 70,000 human deaths.[18] In 1997, *E. histolytica* was reclassified into two species: *E. histolytica* and *Entamoeba dispar* (nonpathogenic); earlier, this differentiation had been difficult to establish because of morphogenetic and phylogenetic similarities.[1,19] This classification is based on the differences in the isoenzyme patterns (zymodemes), the detection of the *E. histolytica*–specific antigen, and *E. histolytica*– and *E. dispar*–specific DNA fragment amplification by polymerase chain reaction (PCR).[3,5]

In Japan, particularly during the last decade, *E. histolytica* infections have not been detected in nonhuman primates by PCR.[12,14] However, three recent articles reported three different pathogenic *E. histolytica*–like variants showing subtle variations in the small-subunit ribosomal RNA (SSU rRNA) gene sequences isolated from cynomolgus monkey (*Macaca fascicularis*),[15] rhesus monkey (*Macaca mulatta*),[13] and De Brazza's guenon (*Cercopithecus neglectus*).[12] The JSK2004-type *E. histolytica* variant (JSK04-Eh-V)[11] has an SSU rRNA gene homology of 99.10% with *E. histolytica* and of 98.47% with *E. dispar*. Previously it was reported that the existing multiplex PCR[2] technique that targeted the specific region of the SSU rRNA gene sequence of *E. histolytica* did not yield the genomic DNA products of an axenic strain (JSK2004) of the *E. histolytica*–like variant from a De Brazza's guenon because of the variation in the nucleotide sequence of the gene.[11]

In the present study, a new multiplex PCR assay that is capable of distinguishing the JSK04-Eh-V

From the Division of Clinical Microbiology, Department of Microbiology, Tokyo Metropolitan Institute of Public Health, 3-24-1, Hyakunin-cho, Shinjuku-ku, Tokyo 169-0073, Japan (Suzuki, Murata, Yanagawa); the Department of Tropical Medicine and Parasitology, School of Medicine, Keio University, 35 Shinanomachi, Shinjuku-ku, Tokyo 160-8582, Japan (Kobayashi, Takeuchi); and the Ueno Zoological Gardens, Ueno-park 9-83, Taito-ku, Tokyo 110-8711, Japan (Tajima, Hashizaki). Correspondence should be directed to Jun Suzuki (Jun_Suzuki@member.metro.tokyo.jp).

Table 1. Oligonucleotide primers used for polymerase chain reaction (PCR) assays in present study.

Primer name		Primer sequence (5′ to 3′)	Nucleotide position	Accession no.
EnthF	(forward)	ATG GCC AAT TCA TTC AAT GA	198–217	X65163
EnthR	(reverse)	TAC TTA CAT AAA GTC TTC AAA ATG T	648–672	X65163
EhvF	(forward)	ATT TTA TAC ATT TTG AAG ACT TTG CA	642–667	AB426549
EhvR	(reverse)	CTC TAA CCG AAA TTA GAT AAC TAC	1466–1489	AB426549
EhvR2	(reverse)	CAG ATT AAG AAA CAA TGC TTC TTC	1052–1075	AB426549
EntdF	(forward)	GTT AGT TAT CTA ATT TCG ATT AGA AC	1467–1492	AB282661
EntdR	(reverse)	ACA CCA CTT ACT ATC CCT ACC TA	1639–1661	AB282661
EchatF	(forward)	AGG ATT TGT TTT ATA ACA AGT TC	471–493	AF149912
EchatR	(reverse)	AAT AAC CTT TCT CCT TTT TCT ATC	660–685	AF149912
EhartF	(forward)	GTG AAG AGA AAG GAT ATC CAA AGT	221–244	AF149907
EhartR	(reverse)	ATA TCA TTT TCA ACT ACG AGC	623–643	AF149907
Chitinase	(forward)	GGA ACA CCA GGT AAA TGT ATA	466–487	U78319
Chitinase	(reverse)	TCT GTA TTG TGC CCA ATT	799–817	U78319
SREHP	(forward)	GCT AGT CCT GAA AAG CTT GAA GAA GCT G	258–286	M80910
SREHP	(reverse)	GGA CTT GAT GCA GCA TCA AGG T	784–806	M80910
R1 (locus1–2)	(forward)	CTG GTT AGT ATC TTC GCC TGT	1–21	AF276055
R2 (locus1–2)	(reverse)	CTT ACA CCC CCA TTA ACA AT	383–401	AF276055

from *E. histolytica* and *E. dispar* was designed, and the prevalence of JSK04-Eh-V infection in the primates of a zoo in Japan was surveyed using this assay. In addition, the identity of the JSK04-Eh-V strains in the zoo, determined by analyzing their polymorphic genotypes as a fingerprint for identifying the strain of *E. histolytica*, was investigated.

Moreover, the incidence of other amoebic infections in primates was investigated, and the first axenic culture medium that would support the growth of *E. histolytica*, JSK04-Eh-V, and *E. dispar* in a single medium was designed.

MATERIALS AND METHODS

Primates

In order to assess the prevalence of infection with JSK04-Eh-V, 47 captive individuals of 11 primate species from the Tokyo Zoo in Japan, where JSK2004 (JSK04-Eh-V) had been isolated from a De Brazza's guenon, were surveyed.[11] The primates, comprising 11 species, included three De Brazza's guenons (*Cercopithecus neglectus*), 11 Abyssinian colobus monkeys (*Colobus guereza*), two ring-tailed lemurs (*Lemur catta*), two mandrills (*Mandrillus sphinx*), one lesser slow loris (*Nycticebus pygmaeus*), two ruffed lemurs (*Varecia variegata*), one northern night monkey (*Aotus trivirgatus*), seven Geoffroy's spider monkeys (*Ateles geoffroyi*), 12 Japanese macaques (*Macaca fuscata*), five white-faced sakis (*Pithecia pithecia*), and one cotton-top tamarin (*Saguinus oedipus*). Each primate species was housed independently.

Microscopic examination and detection of the *E. histolytica*–specific antigen

Stool samples from each living individual were collected once daily for 3 days from 45 primates to obtain three samples per individual. Prior to performing the multiplex PCR, all stool specimens were examined microscopically after concentrating the *Entamoeba* cysts by the formalin–ether sedimentation technique.[10] The specimens were also examined using an *E. histolytica*–specific antigen detection kit (*E. histolytica II* kit; TechLab, Blacksburg, Virginia 24060, USA). Tissue samples obtained from the primates that had liver abscesses were embedded in paraffin, stained with periodic acid–Schiff, and were examined for amoebae.

DNA preparation

Of the three stool specimens collected from each individual, the specimen that had the largest number of amoebic cysts was utilized for DNA preparation. The cysts were concentrated and partially purified using the modified formalin–ether sedimentation method, in which formalin was replaced with a phosphate-buffered solution (pH 7.4). Subsequently, the QIAamp® DNA stool mini-kit (Qiagen GmbH, Hilden 40724, Germany; catalog no. 51504) was used to isolate the genomic DNAs of amoebae. The genomic DNAs of the amoebae found in the two samples of abscesses obtained from the liver abscess of both the autopsied Abyssinian colobus monkey and Geoffroy's spider monkey that died of amoebic liver abscess; the two ref-

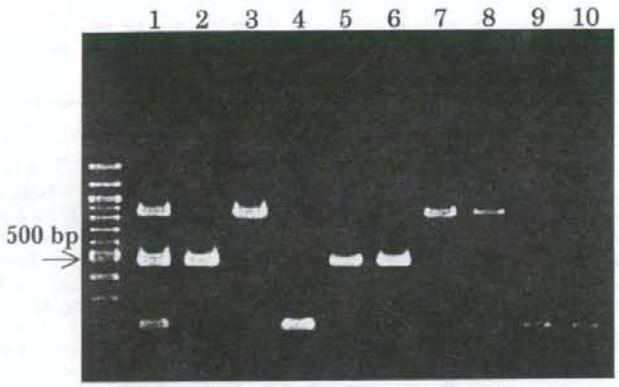

Figure 1. Polymerase chain reaction (PCR) products of the DNA samples from *Entamoeba histolytica*, JSK2004-type *E. histolytica*–like variant (JSK04-Eh-V), and *Entamoeba dispar* differentiated by multiplex PCR. Lane 1: mixture of the DNA templates of lanes 2, 3, and 4; Lane 2: DNA of HM-1:IMSScl6 (*E. histolytica*; length, 475 base pairs [bp]); Lane 3: DNA of JSK2004 clone 2 (JSK2004cl2; JSK04-Eh-V; length, 848 bp); Lane 4: DNA of SAW1734RclAR (*E. dispar*; length, 195 bp); Lane 5: Human *E. histolytica* DNA sample (pus from liver abscess); Lane 6: Human *E. histolytica* DNA sample (stool); Lane 7: JSK04-Eh-V DNA sample (pus from liver abscess) from a Geoffroy's spider monkey; Lane 8: JSK04-Eh-V DNA sample (stool) from a De Brazza's guenon; Lane 9: Human *E. dispar* DNA sample (stool); and Lane 10: *E. dispar* DNA sample (stool) from a De Brazza's guenon.

erence amoebic strains, HM-1:IMSS clone 6 (HM-1:IMSScl6 strain; *E. histolytica*) and SAW1734R clone AR (SAW1734RclAR strain; *E. dispar*), that were kindly supplied by Dr. Lois S. Diamond (National Institutes of Health); and the JSK2004 clone 2 (JSK2004cl2; JSK04-Eh-V) were isolated using the QIAamp DNA mini-kit (Qiagen GmbH; catalog no. 51304).

Primers for multiplex PCR

The primers for multiplex PCR were designed based on the two SSU rRNA gene sequences of HM-1:IMSScl6 (*E. histolytica*; GenBank accession no. X65163) and SAW1734RclAR (*E. dispar*; GenBank accession no. AB282661) and the previously reported sequence of JSK2004cl2 (JSK04-Eh-V; GenBank accession no. AB426549). The three primer sets that were designed—EnthF/EnthR for *E. histolytica*, EntdF/EntdR for *E. dispar*, and EhvF/EhvR for JSK04-Eh-V—are listed in Table 1.

Primer specificity was tested by conducting multiplex PCR on seven other intestinal parasitic protozoan and one nonprotozoan species: axenic trophozoites of *Entamoeba moshkovskii* (Laredo strain), *Entamoeba invadens* (IP-1 strain; ATCC no. 30994), and *Giardia intestinalis* (Portland-1 strain; ATCC no. 30888); cyst forms of *Escherichia coli* and *Cryptosporidium hominis*; culture form of *Blastocystis hominis* (nonprotozoan species) from human stool samples; and *E. coli*, *Entamoeba chattoni*, and *Entamoeba hartmanni* obtained from the stool samples of nonhuman primates.

Multiplex PCR

Amplification was performed in a reaction mixture (50 μl) containing 100 ng of the DNA samples, 25 μl of 2× Multiplex PCR Master Mix (Qiagen GmbH; catalog no. 206143), and 2 μl of each primer at 10 mM. The touchdown method was used for thermal cycling. The cycling conditions were as follows: 15 min at 95°C followed by 40 cycles of denaturation at 94°C for 30 sec, annealing for 40 sec beginning at 61°C and ending at 56°C, and extension at 72°C for 1 min. The annealing temperature was lowered by 1°C after every four cycles until it reached 56°C, after which the same temperature was maintained until the end of the cycling process.

Semi-nested PCR for SSU rRNA

In cases in which a minimal PCR product from the DNA of JSK04-Eh-V was obtained, a semi-nested PCR using the primer set EhvF/EhvR2 was performed (Table 1). For this second PCR (semi-nested PCR), amplification was performed in a reaction mixture (50 μl) containing 1 μl of the first PCR product, 1.0 U of ex*Taq*DNA polymerase (Takara Bio, Inc., Seta, Shiga 520-2134, Japan; catalog no. RR001A), 0.4 μM of each primer, and 0.25 mM of deoxynucleoside triphosphate. The follow-

Table 2. The results of the surveillance for the prevalence of the JSK2004 type *Entamoeba histolytica*-like variant (JSK04-Eh-V) by a newly designed multiplex polymerase chain reaction (PCR) and microscopic examination in a zoo of Tokyo, Japan.

Primate species	Common name	No. of samples	Positive number by multiplex PCR (symptoms)			Antigen detection[a]	Microscopic examination[b]
			Entamoeba histolytica	JSK04-Eh-V	*Entamoeba dispar*		
Old World monkeys							
Cercopithecus neglectus	De Brazza's guenon	3	0	1 (Asymptomatic)	2	1	*E. coli* (3), *E. nana* (2)
Colobus guereza	Abyssinian colobus	11	0	2 (ALA,[c] asymptomatic)	2	1	*E. coli* (8), *E. nana* (3), *G. intestinalis* (4)
Macaca fuscata	Japanese macaque	12	0	0	2	0	*E. chattoni* (7), *E. coli* (2), *E. hartmanni* (5)
Mandrillus sphinx	Mandrill	2	0	0	0	0	*E. chattoni* (1), *E. nana* (1)
Lemur catta	Ring-tailed lemur	2	0	0	0	0	*G. intestinalis* (2)
Varecia variegata	Ruffed lemur	2	0	0	0	0	—
Nycticebus pygmaeus	Lesser slow loris	1	0	0	0	0	—
New World monkeys							
Aotus trivirgatus	Northan night monkey	1	0	0	0	0	*C. mesnili* (1)
Ateles geoffroyi	Geoffroy's spider monkey	7	0	1 (Colitis)	1	0	—
Pithecia pithecia	White-faced saki	5	0	2 (ALA,[c] asymptomatic)	1	2	*G. intestinalis* (1), *E. coli* (1), *E. nana* (1)
Saguinus oedipus	Cotton-top tamarin	1	0	0	0	0	—
Total		47	0	6	8	4	

[a] *E. histolytica*-specific antigen detection kit [*E. histolytica II* kit (TechLab)] was used for examination of stool samples.

[b] *E. coli*: *Entamoeba coli*; *E. nana*: *Endolimax nana*; *G. intestinalis*: *Giardia intestinalis*; *E. chattoni*: *Entamoeba chattoni*; *C. mesnili*: *Chilomastix mesnili*. *E. chattoni* and *E. hartmanni* were identified by PCR. The numbers within the parentheses represent the number of positive cases..

[c] ALA, amebic liver abscess (death).

Figure 2. Differentiated polymerase chain reaction (PCR) products of the DNA samples of *Entamoeba chattoni* and *Entamoeba hartmanni* using PCRs. Lane 1: The product (length, 215 base pairs [bp]) from an *E. chattoni* DNA sample (stool) from a mandrill; Lane 2: The product (length, 215 bp) from an *E. chattoni* DNA sample (stool) from a Japanese macaque; Lane 3: The product (length, 423 bp) from an *E. hartmanni* DNA sample (stool) from a Japanese macaque.

ing cycling parameters were utilized: *Taq* activation at 94°C for 3 min; 35 cycles of denaturation at 94°C for 40 sec, annealing at 58°C for 40 sec, and extension at 72°C for 1 min; and extension at 72°C for 5 min.

PCR for *E. chattoni* and *E. hartmanni*

Entamoeba chattoni and *E. hartmanni* were identified by PCR assays using two primer sets (i.e., EchatF/EchatR[16] and EhartF/EhartR, respectively) (Table 1). For *E. hartmanni*, a newly designed primer set based on its SSU rRNA sequence (GenBank accession no. AF149907) was used. These amplifications were performed in a reaction mixture (50 μl) containing 100 ng of the DNA sample, 1.0 U of LA*Taq*DNA polymerase, 0.4 μM of each primer, and 0.25 mM of deoxynucleoside triphosphate. The following cycling parameters were utilized: *Taq* activation at 94°C for 3 min; 35 cycles of denaturation at 94°C for 40 sec, annealing at 55°C for 40 sec, and extension at 72°C for 1 min; and extension at 72°C for 5 min.

Polymorphic gene analysis

The genotyping of JSK04-Eh-V was reexamined to determine whether it would have the same genotype as JSK2004cl2. This was performed based on the nucleotide sequences of two protein-coding (chitinase and SREHP) genes and the protein-noncoding locus 1-2[4,7,20] that was used as a fingerprint for identifying the *E. histolytica* strain. The primers used are shown in Table 1. These amplifications were performed in a reaction mixture (50 μl) containing 100 ng of the DNA sample, 1.0 U of LA*Taq*DNA polymerase (Takara Bio, Inc.; catalog no. RR02AG), 0.4 μM of each primer, and 0.25 mM of deoxynucleoside triphosphate. The following cycling parameters were utilized: *Taq* activation at 94°C for 3 min; 35 cycles of denaturation at 94°C for 40 sec, annealing at 50°C (chitinase, SREHP, and locus 1-2) or 56°C (SSU rRNA) for 40 sec, and extension at 72°C for 1 min; and extension at 72°C for 5 min.

Sequence analysis

Sequence analysis was performed. The multiplex PCR products of SSU rRNA; the PCR products of chitinase, SREHP, and the locus 1-2 genes from the JSK04-Eh-V isolates; and the PCR products of SSU rRNA from *E. chattoni* and *E. hartmanni* were sequenced using the ABI Prism BigDye Terminator v3.1 Cycle Sequencing Ready Reaction Kit (Applied Biosystems, Foster City, California 94404, USA; catalog no. 4337455) and an ABI PRISM 3100 Genetic Analyzer.

Yeast extract–iron–maltose–dihydroxyacetone–serum (YIMDHA-S) medium

An axenic culture medium, namely, YIMDHA-S, based on the yeast extract–iron–gluconic acid–dihydroxyacetone–serum medium (YIGADHA-S)[6] designed for the axenic culture of *E. dispar*, was designed for the isolation and culture of *E. histolytica*, the *E. histolytica*–like variant, and *E. dispar* in a single medium. YIGADHA-S differs from the existing YIMDHA-S medium in that gluconic acid, 0.5% in YIGADHA-S, is replaced with an equal concentration of maltose in YIMDHA-S. Another significant issue related to this culture system is that the growth of amoebae in YIMDHA-S is largely affected by the quality of the yeast extract. Accordingly, the effectiveness of several commercially available yeast extracts purchased from different manufacturers as an ingredient of YIMDHA-S was evaluated. Except for the standard stock obtained from BBL (Becton Dickinson Co., Cockeysville, Maryland 21030, USA; catalog no. 4311929; lot no. 1000I9DHJT), among all the yeast extracts test-

Figure 3. Comparison of the chitinase sequences of the *Entamoeba histolytica*–like variant strain JSK2004cl2 and *E. histolytica*–like variants detected from *Ateles geoffroyi* and *Pithecia pithecia* with the sequences of the reference *E. histolytica*–like variant strain isolated from *Macaca fascicularis*. JSK2004cl2: The sequence of the chitinase gene of DNA from JSK2004cl2 obtained from a De Brazza's guenon (GenBank accession no. AB426705). *Samples: The chitinase gene sequences of DNA samples from a Geoffroy's spider monkey (one pus sample from a liver abscess) and white-faced saki (two stool samples); EHMfas1: the chitinase gene sequences (GenBank accession no. AB282755) of the DNA of an isolate of another type of *E. histolytica*–like variant isolated from a cynomolgus monkey.[15]

ed, only that obtained from Merck (Merck KGaA, Damstadt 64271, Germany; catalog no. 1.03753; lot no.VM510453 539) was effective for constant subculture of the axenic strains of *E. histolytica* (HM-1:IMSScl6), *E. dispar* (AS16 IR isolated from human samples and CYNO 09:TPC isolated from the cynomolgus monkey [*Macaca fascicularis*]),[6] and JSK04-Eh-V (JSK2004) from the De Brazza's guenons that were subjected to a trial of axenic cultivation.

RESULTS

Specificity of multiplex PCR

Each PCR product from the genomic DNA of each of the axenic strains of *E. histolytica* (HM-1: IMSScl6), JSK04-Eh-V (JSK2004cl2), and *E. dispar* (SAW1734clAR) analyzed by multiplex PCR was obtained independently; the lengths of the fragments were 475 base pairs (bp), 848 bp, and 195 bp, respectively (Fig. 1), which was confirmed by individual nucleotide sequencing. The findings of multiplex PCR were reproducible during the practical trials using amoebic DNAs isolated from the stool samples and liver abscesses of humans and nonhuman primates infected with *E. histolytica*, JSK04-Eh-V, and *E. dispar* (Fig. 1). The specificity of multiplex PCR was examined by analyzing the templates of the DNA extracted from seven other intestinal parasitic protozoan and one nonprotozoan species, as previously described. None of the PCR products was observed on multiplex PCR examination of these parasites.

Sensitivity of multiplex PCR and semi-nested PCR

The sensitivity of multiplex PCR was found to be at least 200 cysts/100 mg of the stool sample for JSK04-Eh-V and 100 cysts/100 mg of the stool samples for *E. histolytica* and *E. dispar*. In an attempt to assess the sensitivity of the technique for mixed infections, 400 cysts or trophozoites of JSK04-Eh-V could be detected and differentiated in the presence of 100 cysts/100 mg of the stool samples for *E. histolytica* and *E. dispar*.

Semi-nested PCR using the primer set EhvF/EhvR2 detected 50 cysts/100 mg stool sample for JSK04-Eh-V. In one case of the white-faced saki, in which a minimal PCR product from the DNA of JSK04-Eh-V was obtained, semi-nested PCR yielded the 434-bp–long PCR product.

```
JSK2004cl2 AAG AAA AAG AAA AAA GTA GCT CAG CAA AAC CAG AAT CAA GTT CAA ACA AAG ATA ATG AAG
EHMfas1     ... ... ... ... ... ... ... ... ... ... ... ... ... ... ... ... ... ... ...
P19         ... ... ... ... ... ... ... ... ... ... ... ... ... ... ... ... ... ... ...

JSK2004cl2 ATG AGG AAG ATG AAG ATG AAG ATG ATG AAG AAG ATG AAG ATG AGA ATG AAA AAG CAA GTT
EHMfas1     ... .-- --- -G. ... ... ... ... ... ... ... ... ... ... ... ... ... ... ...
P19         ..A .-- --- -.. ... ..A .T. .A. ... .G. ... ... ... ... ... ... ... ... ...

JSK2004cl2 CAA GTG ATA AAT CAG AAG CAA GTT CAA GTG ATA AAT CAG A--- --- --- --- -AT CAA GCT
EHMfas1     ... ... ... ... ... ... ... ... ... ... ... ..C ... .TA ACA AAC CAG A.G ... ...
P19         ... ... ... ... ... ... ... .C. ... ... ... ..C ... .--- --- --- --- -.G ... .T.

JSK2004cl2 CAA ATG ATA AAT CAG AAT CAA GCT CAA ATG ATA AAC CAG AAT CAA GCT CAA ATG ATA AAC
EHMfas1     ... G.. ... ..C ... ..G ... ... ... G.. ... ... ... ..G ... .T. ... G.. ... ...
P19         ... G.. ... ..C ... ..G ... .T. ... G.. ... ... ... ..G ... .T. ... G.. ... ...

JSK2004cl2 CAG AAG CAA GTT CAA GTG ATA AAT CAG AAG CAA GTT CAA GTG ATA AAC CAG ATA ACA AAC
EHMfas1     ... .-- --- --- --- -.A .C. ..C ... ... ... ... ... ... ... ... ... ... ...
P19         ... .-- --- --- --- -.A .C. ..C ... ... ... ... ... ... ... ... ... ... ...

JSK2004cl2 CAG AAG CAA GTT CAA GTG ATA AAC CAG ATA ACA AAC CAG AAG CAA GTT CAA GTG ATA AAC
EHMfas1     ... ... ... .G. ... ... ... ... ... ... ... ... ... ... ... ... ... ... ...
P19         ... ... ... ... ... ... ... ... ... ... ... ... ... ... ... .C. ... ... ...

JSK2004cl2 CAG ATA ACA AAC CAG AAG CAA GTT CAA GTG ATA AGC CAG ATA ACA AAC CAG AAG CAA GCT
EHMfas1     ... ... ... ... ... ... ... .C. ... ... ... .A. ... ... ... ... ... ... ...
P19         ... ... ... ... ... ... ... .C. ... ... ... .A. ... ... ... ... ... ... .T.

JSK2004cl2 CAA CTA ATA AAC CAG AAG CAA GTT CAA CTA ATA AAC CAG AAG CAA GTT CAA CTA GTA ATT
EHMfas1     ... ... ... ... ... ... ... ... ... ... ... ... ... ... ... ... ... ... ...
P19         ... ... ... ... ... ... ... ... ... ... ... ... ... ... ... ... ... ... ...

JSK2004cl2 CAA -TG ATA AAT CAG AAA GTA GTT CAG ATA ATG ATA ATA ATA (GenBank.:AB426706)
EHMfas1     ... A.. ... ... ... ... ... ... ... ... ... ... ... ... ... (GenBank.:AB197935)
P19         ... A.. ... ... ... ... ... ... ... ... ... ... ... ... ... (GenBank :AB282662)
```

Figure 4. Comparison of the sequences in the SREHP of the *Entamoeba histolytica*–like variant JSK2004cl2 strain with the reference *E. histolytica*–like variant strains isolated from *Macaca fuscicularis* and *Macaca mulatta*. JSK2004cl2: The sequence of the serine-rich *E. histolytica* protein (SREHP) gene in the DNA of JSK2004cl2 from a De Brazza's guenon (GenBank accession no. AB426706); EHMfas1: the sequences of the SREHP gene (GenBank accession no. AB197935) in the DNA of an isolate of another type of *E. histolytica*–like variant isolated from a cynomolgus monkey;[15] P19: the sequence of the SREHP gene (GenBank accession no. AB282662) in the DNA of another type of *E. histolytica*–like variant (an established strain) isolated from a rhesus monkey.[13]

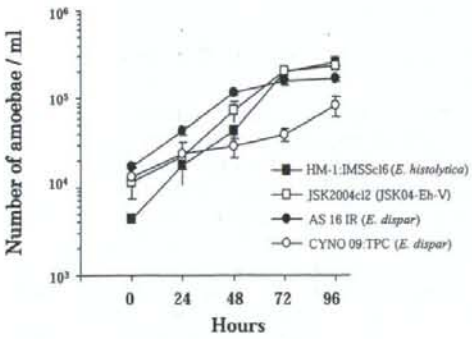

Figure 5. The growth kinetics of the axenically cultured HM-1:IMSScl6, JSK2004cl2, AS 16 IR, and CYNO 09:TPC strains in the yeast extract–iron–maltose–dihydroxyacetone–serum (YIMDHA-S) medium. The mean numbers of amoebae in duplicate cultures have been plotted.

Prevalence of amoebic infections in the zoo

Since a pathogenic JSK04-Eh-V strain was isolated from De Brazza's guenons in the Tokyo zoo, the prevalence of JSK04-Eh-V infection was surveyed using multiplex PCR and was detected in six individuals of four primate species: Abyssinian colobus monkey; De Brazza's guenon, including the individual from which JSK2004 was isolated; white-faced saki; and Geoffroy's spider monkey. In addition, the autopsied samples of the Abyssinian colobus monkey and Geoffroy's spider monkey that died of amoebic liver abscess were positive for JSK04-Eh-V. Among the primates of the zoo, the infection rates with *E. histolytica*, *E. dispar*, and JSK04-Eh-V were 0% (0/47), 17% (8/47), and 13% (6/47), respectively (Table 2). Mixed infection with *E. dispar* and JSK04-Eh-V was not detected by multiplex PCR. The prevalence of the other species of amoebae examined microscopically (i.e., *E. coli* and *Endolimax nana*), were 30% (14/47) and 15%

(7/47), respectively. The prevalence of *E. chattoni* and *E. hartmanni* examined microscopically and by PCR was 17% (8/47) and 11% (5/47), respectively (Table 2); their fragments were confirmed by nucleotide sequencing and corresponded to the sequence dates of *E. hartmanni* (GenBank accession no. AF149907) and *E. chattoni* (GenBank accession no. AF149912). The amplified PCR products are shown in Figure 2.

Polymorphic genes in JSK04-Eh-V isolates

Genotyping based on the nucleotide sequencing of the chitinase, SREHP, and locus 1-2 genes was applied to the genotyping of JSK04-Eh-V. The DNA samples of JSK04-Eh-V from each of the six primates were subjected to PCR to detect the fragments of the chitinase, SREHP, and locus 1-2 genes. The PCR products of the chitinase genes from the DNA samples of two primates and JSK2004cl2 and the PCR products of the locus 1-2 genes from the DNA samples of four primates and JSK2004cl2 were sequenced; however, the PCR products of the SREHP genes were obtained only from the DNA sample of JSK2004cl2. There was perfect homology between the sequences of the PCR products of the chitinase genes obtained from two primates (one Geoffroy's spider monkey and one white-faced saki) and the PCR products of the locus 1-2 genes from four primates (two Abyssinian colobus monkeys, one Geoffroy's spider monkey, and one white-faced saki). Moreover, the sequences of the two genes of JSK2004cl2 (locus 1-2: GenBank accession no. AB426704; chitinase: GenBank accession no. AB426705) also demonstrated perfect homology. However, the sequence data of the chitinase and SREHP genes of the other two types of *E. histolytica*–like variants (GenBank accession nos. AB282755 and AB197935) isolated from the cynomolgus and rhesus monkeys were different compared to the sequence data of the chitinase gene and SREHP gene (GenBank accession no. AB426706) of JSK2004cl2 (Figs. 3, 4).

Growth kinetics of amoebae in YIMDHA-S

The growth kinetics of axenically grown *E. histolytica* (HM-1:IMSScl6), *E. dispar* (AS 16 IR and CYNO 09:TPC), and JSK04-Eh-V (JSK2004) in YIMDHA-S are shown in Figure 5. These established axenic strains adapted to the YIMDHA-S culture conditions within three subcultures; thereafter, they were inoculated into the YIMDHA-S from the classic TYI-S-33[3] (HM-1:IMSScl6) or YIGADHA-S (AS 16 IR and CYNO 09:TPC) media.

DISCUSSION

The multiplex PCR for *E. histolytica*, JSK04-Eh-V, and *E. dispar* permits species identification in a single reaction mixture and is, therefore, more cost effective and useful for prevention of contamination of DNA samples.

Surveillance of the prevalence of JSK04-Eh-V infection among the primates in the zoo was conducted using multiplex PCR for differential diagnosis of *E. histolytica*, JSK04-Eh-V, and *E. dispar*. Multiplex PCR was confirmed as a useful method for the detection and identification of *E. histolytica*, JSK04-Eh-V, and *E. dispar* in nonhuman primates and even in the zookeepers who were in contact with the primates, because the specificity and reproducibility of this technique were adequate for efficient surveillance of JSK04-Eh-V in the present study.

Concerning the microscopic stool examination process in this survey, amoebic cysts or trophozoites were not always detected in every stool sample obtained from individuals infected with JSK04-Eh-V and *E. dispar*. These cysts or trophozoites could be detected only in one third to two thirds of the stool samples, despite the collection of samples from each individual primate once a day for 3 days. The results indicated that performing a stool examination per day (at least three times) on alternate days is necessary.

The JSK04-Eh-V strain of *E. histolytica* was detected by using the *E. histolytica II* kit, an *E. histolytica*–specific antigen (adhesin) detection kit. It is reported that one of the factors determining the pathogenicity of *E. histolytica* is the cytolysis of host cells that begins with the adhesion of the amoebae to the mucosal target cells of the large intestine via galactose/*N*-acetyl D-galactosamine-inhibitable (Gal/GalNAc) lectin.[8,9] The detection of the *E. histolytica*–specific antigen from JSK04-Eh-V by using the *E. histolytica II* kit indicated that the Gal/GalNAc lectin structure in JSK04-Eh-V is identical to that in *E. histolytica*.

Although the nucleotide sequence of the polymorphic SREHP gene from five primates, except for JSK2004cl2, could not be amplified by PCR, the polymorphic chitinase and locus 1-2 gene sequences from three and six primates, respectively, were observed to be identical. The reasons for the inability of PCR to amplify the SREHP gene were thought to be related to the small amount of JSK04-Eh-V DNA in the stool and liver abscess samples, which were insufficient for the PCR, and the presence of a few irrelevant PCR fragments in each case. Therefore, JSK04-Eh-V infections that oc-

curred in the zoo was presumed to have been spread by a single strain, because the infection was limited to primate groups within a particular zone of the zoo at around the same time. The route of transmission of the infection from the isolated group of primates in captivity, including individuals infected with JSK04-Eh-V, to the other groups has not been determined. It is possible that the cysts are the causative agents of JSK04-Eh-V infection, because *E. histolytica* cysts have been reported to be capable of surviving and retaining their infectivity for a month under appropriate wet conditions.[17]

The symptoms of the zoo primates infected with JSK04-Eh-V differed considerably depending on their species; the symptoms in the De Brazza's guenon were relatively mild, while symptoms in the Abyssinian colobus monkey and Geoffroy's spider monkey were severe and fatal. There appear to be species-specific differences among the primates with regard to susceptibility. Although the transmission route was not clear, it is possible that the primates may be carriers and may thus be a source of the parasite. Prior to this study, JSK04-Eh-V infection was thought to have been eradicated, owing to the diligence of the veterinarians and zookeepers working in the zoo, and, fortunately, no zoonotic infection (including amoebiasis) was found among the zookeepers.

YIMDHA-S was designed for the axenic culture of *E. histolytica*, JSK04-Eh-V, and *E. dispar*. This medium is considered to be efficient in comparing biological characteristics of JSK04-Eh-V with *E. histolytica* and *E. dispar*, such as the intensity of in vitro virulence to mammalian tissue culture cell lines,[9] in a single medium under the same culture conditions.

Acknowledgment: A part of this work was supported by a Health Sciences Research Grant-in-Aid for Emerging and Reemerging Infectious Diseases from the Ministry of Health, Labour and Welfare of Japan.

LITERATURE CITED

1. Diamond, L. S., and C. G. Clark. 1993. A redescription of *Entamoeba histolytica* Schaudinn, 1903 (Emended Walker, 1911) separating it from *Entamoeba dispar* Brumpt, 1925. J. Eukaryot. Microbiol. 40(3): 340–344.

2. Diamond, L. S., D. R. Harlow, and C. C. Cunnick. 1978. A new medium for the axenic cultivation of *Entamoeba histolytica* and other *Entamoeba*. Trans. R. Soc. Trop. Med. Hyg. 72(3): 431–432.

3. Evangelopoulos, A., G. Spanakos, E. Patsoula, N. Vakalis, and N. Legakis. 2000. A nested, multiplex, PCR assay for the simultaneous detection and differentiation of *Entamoeba histolytica* and *Entamoeba dispar* in faeces. Ann. Trop. Med. Parasitol. 94: 233–240.

4. Ghosh, S., M. Frisardi, L. Ramirez-Avila, S. Descoteaux, K. Sturm-Ramirez, O. A. Newton-Sanchez, J. I. Santos-Preciado, C. Ganguly, A. Lohia, S. Reed, and J. Samuelson. 2000. Molecular epidemiology of *Entamoeba* spp.: evidence of a bottleneck (demographic sweep) and transcontinental spread of diploid parasites. J. Clin. Microbiol. 38: 3815–3821.

5. Haque, R., I. K. Ali, S. Akther, and W. A. Petri, Jr. 1998. Comparison of PCR, isoenzyme analysis, and antigen detection for diagnosis of *Entamoeba histolytica* infection. J. Clin. Microbiol. 36: 449–452.

6. Kobayashi, S., E. Imai, A. Haghighi, S. A. Khalifa, H. Tachibana, and T. Takeuchi. 2005. Axenic cultivation of *Entamoeba dispar* in newly designed yeast extract-irongluconic acid-dihydroxyacetone-serum medium. J. Parasitol. 91: 1–4.

7. Li, E., C. Kunz-Jenkins, and S. L. Stanley, Jr. 1992. Isolation and characterization of genomic clones encoding a serine-rich *Entamoeba histolytica* protein. Mol. Biochem. Parasitol. 50(2): 355–357.

8. Petri, W. A., Jr., R. D. Smith, P. H. Schlesinger, C. F. Murphy, and J. I. Ravdin. 1987. Isolation of the galactose-binding lectin that mediates the in vitro adherence of *Entamoeba histolytica*. J. Clin. Invest. 80: 1238–1244.

9. Ravdin, J. I., and R. L. Guerrant. 1982. Separation of adherence, cytolytic, and phagocytic events in the cytopathogenic mechanisms of *Entamoeba histolytica*. Arch. Invest. Med. 13: 123–128.

10. Ritchie, L. S. 1948. An ether sedimentation technique for routine stool examinations. Bull. U. S. Army Med. Dept. 8: 326.

11. Suzuki, J., S. Kobayashi, R. Murata, Y. Yanagawa, and T. Takeuchi. 2007. Profile of a pathogenic *Entamoeba histolytica*-like variant with variations in the nucleotide sequence of the small subunit ribosomal RNA isolated from a primate (De Brazza's Guenon). J. Zoo Wildl. Med. 38(3): 471–474.

12. Tachibana, H., X. J. Cheng, S. Kobayashi, N. Matsubayashi, S. Gotoh, and K. Matsubayashi. 2001. High prevalence of infection with *Entamoeba dispar*, but not *E. histolytica*, in captive macaques. Parasitol. Res. 87: 114–117.

13. Tachibana, H., T. Yanagi, K. Pandey, X. J. Cheng, S. Kobayashi, J. B. Sherchand, and H. Kanbara. 2007. An *Entamoeba* sp. strain isolated from rhesus monkey is virulent but genetically different from *Entamoeba histolytica*. Mol. Biochem. Parasitol. 153(2): 107–114.

14. Takano, J., T. Narita, H. Tachibana, T. Shimizu, H. Komatsubara, K. Terao, and K. Fujimoto. 2005. *Entamoeba histolytica* and *Entamoeba dispar* infections in cynomolgus monkeys imported into Japan for research. Parasitol. Res. 97: 255–257.

15. Takano, J., T. Narita, H. Tachibana, K. Terao, and K. Fujimoto. 2007. Comparison of *Entamoeba histolytica* DNA isolated from a cynomolgus monkey with human isolates. Parasitol. Res. 101(3): 539–546.

16. Verweij, J. J., A. M. Polderman, and C. G. Clark. 2001. Genetic variation among human isolates of uninu-

cleated cyst-producing *Entamoeba* species. J. Clin. Microbiol. 39(4): 1644–1646.

17. Walsh, J. A. 1988. Transmission of *Entamoeba histolytica* infection. *In:* Amebiasis. Wiley Medical, John Wiley and Sons, Inc., New York, New York. Pp. 106–126.

18. World Health Organization. 1995. The World Health Report 1995: Bridging the Gaps, vol. 16. World Health Organization, Geneva, Switzerland. Pp. 28–29.

19. World Health Organization. 1997. Amoebiasis. W. H. O. Wkly. Epidemiol. Rec. 72: 97–100.

20. Zaki, M., and C. G. Clark. 2001. Isolation and characterization of polymorphic DNA from *Entamoeba histolytica*. J. Clin. Microbiol. 39(3): 897–905.

Received for publication 12 December 2007